Effect of the Choice of the Pressure Coupling Method on the Spontaneous Aggregation of DPPC Molecules

Ronak Y. Patel and Petety V. Balaji*

School of Biosciences and Bioengineering, Indian Institute of Technology Bombay, Powai, Mumbai 400 076, India

Received: May 23, 2005; In Final Form: June 14, 2005

The self-assembly of DPPC molecules starting from a random, solution-like configuration in the presence of water molecules is described in the present MD simulation study. Simulations were performed with either anisotropic or isotropic pressure coupling. Use of anisotropic pressure coupling led to the formation of a bilayer/bilayerlike aggregate; the features of the bilayer are in agreement with those reported from earlier simulation and experimental studies. In contrast, simulating the same system with isotropic pressure coupling led to the formation of a cylindrical micelle/lamellar structure with a large water hole. The formation of micelles seems unrealistic since diacylphosphatidylcholines having hydrocarbon tails with nine or more carbon atoms have been shown to form only bilayers. Simulations were also performed with preformed bilayerlike configurations with either anisotropic or isotropic pressure coupling. The bilayer characteristics deduced from simulations using anisotropic pressure coupling are in better agreement with those reported from earlier experimental and simulation studies. Thus, the choice of the pressure coupling method has a significant effect on the spontaneous aggregation of DPPC molecules but makes relatively lesser effect if the bilayer has formed already.

Introduction

Biological membranes are phospholipid aggregates containing a variety of embedded constituents and are of fundamental importance in biology. These aggregates are characterized by lateral, rotational and flip-flop mobility of the constituent phospholipids. This compositional and motional heterogeneity has made the characterization of their structure and dynamics a nontrivial task. A number of biophysical techniques and MD simulations have been used to study the structure, dynamics and interactions of model and biological membranes,[1−10] to characterize preformed aggregates with or without embedded guest molecules,[11−15] and to study the self-assembly of phospholipids.[16−18]

The accuracy and reliability of MD simulation results are critically dependent on the choice of the simulation parameters. The effects of macroscopic boundary conditions, water model, charges, Lennard-Jones interaction parameters between carbons and water,[19] different treatments of electrostatic interactions, time step for the integration of equation of motion, and the pressure algorithm[20] have all been evaluated. A comparative study of simulations in *NVT* and *NPT* ensembles showed that simulations in the *NVT* ensemble lead to lower minimum density at the center of the bilayer than those in the *NPT* ensemble; the latter gave results that are closer to the experimental values.[19] In another study, it was found that truncating electrostatic interactions using cutoffs leads to lower area per lipid and enhanced order of acyl chains compared to using the PME approach; pronounced maxima or minima in radial distribution function were observed exactly at the cutoff distance indicating artificial ordering.[21]

The simulation system can be maintained at constant pressure isotropically, semi-isotropically or anisotropically:[20] (a) In isotropic coupling, all the three unit-cell dimensions are scaled equally and simultaneously ($Np_{sys}T$). (b) In the case of semi-isotropic coupling (Np_Np_LT), the system is coupled to pressure bath independently along bilayer normal (Z axis) and plane (X/Y axis). (c) In the case of anisotropic pressure ($Np_Xp_Yp_ZT$) coupling, all the three unit-cell dimensions are scaled independently while maintaining the total pressure constant. It was observed that the structure and dynamics of hydrated DPPC are not much affected by coupling system either with semi-isotropic or anisotropic pressure; even the choice of pressure coupling algorithm (Parrinello−Rahman or Berendsen) did not have any significant effect on the equilibrium properties of the bilayer.[20]

A number of MD simulation studies on the spontaneous assembly of lipid molecules have been reported.[16−18,22−26] Some studies have used isotropic pressure coupling,[16,25] whereas others have used either semi-isotropic[17] or anisotropic[22] pressure coupling to maintain constant pressure. In these studies, the nature and number of lipid molecules simulated (e.g., 54 DPC, 64 or 1017 DPPC, and 128 DOPC + DOPE) are different so also the nature of assembly that is formed by these lipid molecules (e.g., spherical micelle, bilayer and vesicle-like). It is not clear if the nature of pressure coupling has in any way influenced the type of assembly that is eventually formed during the simulations. In view of this, in the present MD simulation study, the self-assembly of DPPC molecules starting from a random configuration has been investigated with isotropic and with anisotropic pressure coupling.

Methods

Generation of Initial Configurations. The coordinates of a single DPPC molecule were generated using standard bond lengths and angles using in-house software. These were used to generate two types of initial configurations, random (**R**) and

* Corresponding author. Telephone: +91−22−25 76 77 78. Fax: +91−22−25 72 34 80. E-mail: balaji@iitb.ac.in.

10.1021/jp052697m CCC: $30.25
Published on Web 07/13/2005

TABLE 1: Summary of the Systems Setup for Simulations[a]

simulation name[b]	no. of water molecules	DPPC:water (rounded off to nearest integer)	box size (nm)	length of simulation (ns)	initial configuration
AR1, IR1	7049	71.9	7.10 × 7.80 × 9.60	26, 7	random
AR2, IR2	6291	64.2	6.75 × 6.75 × 6.75	20, 20	random
AR3, IR3	6295	64.2	6.75 × 6.75 × 6.75	7, 7	random
AR4, IR4	6572	67.1	6.90 × 6.90 × 6.90	10, 10	random
AR5, IR5	6564	67.0	6.90 × 6.90 × 6.90	7, 7	random
ABN, IBN	6713	68.5	5.60 × 5.60 × 12.0	11, 11	bilayerlike
ABI, IBI	6927	70.6	5.50 × 5.40 × 12.0	11, 11	bilayerlike

[a] All the simulations systems had 98 DPPC molecules. In systems which had bilayerlike configuration initially, each of the two monolayers had 49 DPPC molecules. [b] The initial **I** and **A** denote isotropic and anisotropic pressure coupling, respectively. **BN**, **BI** and **R** refer to the initial configuration of DPPC molecules and denote bilayerlike, noninterdigitating hydrocarbon chains (**BN**), bilayerlike, interdigitating hydrocarbon chains (**BI**) and randomly oriented DPPC molecules (**R**). Five different random configurations were simulated (**R1**−**R5**). The **BN** and **BI** systems differ in the initial conformation of the choline headgroup besides being different in the hydrocarbon interface region between the two monolayers. The ball-and-stick representations of the initial **BN** and **BI** configurations are shown in Figure S1.

bilayerlike (**B**). The total number of DPPC molecules is 98 in both the cases. To generate the random configuration **R**, DPPC molecules were rigid-body rotated and translated randomly within a box of prespecified size. Five different configurations with randomly oriented DPPC molecules were generated and are denoted **R1**−**R5** (Table S1).

To generate a bilayerlike configuration, a single molecule of DPPC was positioned at the origin of a frame of reference in such a way that the long-axis of the molecule is along the *Z* axis of the simulation box. This DPPC molecule was rotated about its own axis by 60° and translated by 0.75 nm along the *X* or the *Y* axis to get a monolayer. The second leaflet of the bilayer was generated in a similar way. Two bilayerlike configurations were generated: in one, the two opposing hydrocarbon chains are inter-digitated (**BI**), and in the other, they were not (**BN**) (Figure S1). The box containing the DPPC molecules in a random or bilayerlike configuration were filled with SPC water molecules. In systems with bilayerlike configuration, water molecules present in the hydrophobic core were deleted.

All seven initial configurations, viz., **R1**−**R5** and **BN** and **BI**, were simulated with either isotropic or anisotropic pressure coupling for various time durations (Table 1). These simulations were identified by prefixing **I** (for isotropic) or **A** (for anisotropic) to the configuration name. Thus, **IR1** and **AR1** refer to simulations performed starting with the **R1** configuration with isotropic and anisotropic pressure coupling, respectively.

Simulations Parameters. The systems generated above were simulated in the *NPT* ensemble with either anisotropic or isotropic pressure coupling (Table 1). Simulations were performed using GROMACS 3.1.4[27,28] run in parallel on an Intel Xeon 2.4 GHz dual processor system under Red Hat Linux 8.0. The bonding and nonbonding parameters are from Berger et al.[29] and the atomic charges are from Chiu et al.[30] The van der Waals interactions were cutoff at 1.2 nm. PME was used for long-range electrostatic interactions since it was found to be better than simple cutoffs;[21,31] the cutoff was set to 1.2 nm for real space calculation. Pressure was coupled either isotropically (equal scaling factor for all three sides) or anisotropically (scaling factor calculated independently for each of the three sides) using Berendsen's algorithm;[32] reference pressure was set to 1 bar, coupling constant to 1 ps and isothermal compressibility to 4.5×10^{-5} bar^{-1}. The temperature was kept constant at 325 K through an external thermostat[32] with a coupling constant of 1 ps. The simulation temperature was chosen such that it is higher than the main transition temperature (viz., 315 K) for DPPC.[10] The bond lengths were constrained using SHAKE. Periodic boundary conditions were applied in all the three directions. The equations of motion were integrated with a time step of 2 fs and the trajectories were saved at 4 ps intervals.

Results

Evolution of the System with Initially Randomly Oriented DPPC Molecules with Isotropic Pressure Coupling. In simulation **IR1**, a rapid segregation of the hydrophobic and hydrophilic groups is observed during the initial 2−3 ns (Figure 1A). The hydrophobic tails come nearer to each other forming an aggregate. The predominantly hydrophobic interior of this aggregate is partly devoid of water molecules. The water molecules, expelled from the interior of this aggregate, are mainly restricted along the *Z* and *Y* directions. The hydrophobic interior of the aggregate interacts with its periodic image along both the positive and negative *X* directions. A continuous hydrophobic core of lipid molecules is thus formed along the *X* direction and the lipid−water contacts are observed along the *Y* and *Z* directions (Figure 1A). On further simulation, the remaining water molecules are also expelled from the interior of the aggregate; this is accompanied by the rearrangement of the water molecules and the polar headgroups at the surface of this aggregate. Overall, these rearrangements result in the consolidation of the hydrophobic core of the aggregate, which now resembles a cylindrical micelle. These rearrangements are completed by 4 ns of simulation; no significant changes are observed on further simulations.

The size of the simulation box remains essentially constant because of isotropic pressure coupling (Figure S2 and Table S2). The formation of the aggregate along the *X* direction does not seem to be a random event; instead, it appears to be related to the differences in the size of the simulation box along the three directions. Being a rectangular parallelepiped, the box is 9.6 nm along the *Z* direction and 7.1 nm along the *X* direction; it is intermediate along the *Y* direction (Table 1).

Simulation **IR4** was performed in a cubic box; a cylindrical micelle is formed in this simulation also, as in simulation **IR1**. The size of the box used for simulation **IR4** is smaller than that used for simulation **IR1** (Table 1), though both simulations were done with 98 DPPC molecules. The dynamics during the initial stages of simulation **IR4** are similar to those observed in **IR1**: rapid segregation of the hydrophobic fatty acyl chains and the water molecules. Subsequently, the molecules rearrange in such a way that the water molecules are mostly restricted to the middle of the simulation box and the fatty acyl chains are toward the edges of the box; thus, the micelle is complete only when the periodic images of the box are considered (Figure 1C).

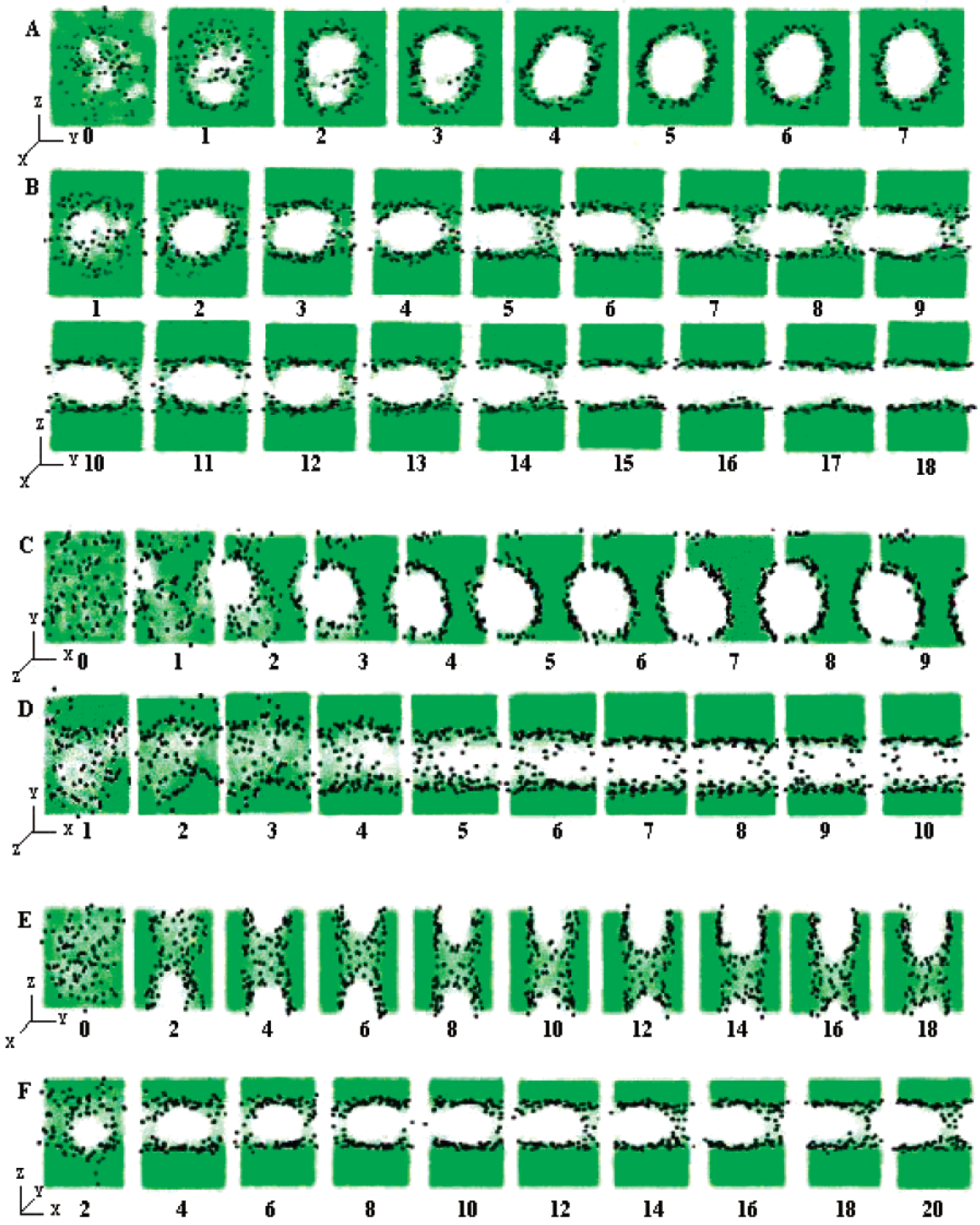

Figure 1. Snapshots showing various stages of aggregation of initially randomly oriented DPPC molecules in simulations **IR1** (panel A), **AR1** (panel B), **IR4** (panel C), **AR4** (panel D), **IR2** (panel E), and **AR2** (panel F). The snapshots were taken at 1 ns intervals for simulations **IR1**, **AR1**, **IR4** and **AR4** and at 2 ns intervals for simulations **IR2** and **AR2**. The time points at which the snapshots were taken are indicated below the respective snapshots. The snapshots have been rendered using VMD.[51] Water molecules are rendered as small spheres and the phosphorus atoms of DPPC are rendered as large spheres; all other atoms of DPPC have been omitted for clarity. The central region appearing white is the hydrophobic interior occupied by the hydrocarbon chains. The coordinate frame is indicated for each panel.

The shape and size of the simulation box used in **IR5** is identical to that used in simulation **IR4**. However, the nature of lipid aggregate formed in this simulation is different from that in **IR4** and is similar to those in simulations **IR2** and **IR3**. The segregation of the hydrophobic and hydrophilic groups occurs rapidly during the initial stages itself (2−3 ns). The arrangement of the lipid and water molecules occurs in such a way that the lipid molecules lose contact with each other in only one direction; this is unlike in **IR1** and **IR4,** wherein the contacts are lost in two directions (Figure 1E). By 5 ns, the lipid molecules rearrange to a lamellar structure with a fairly large water channel; the diameter at the center of this water channel is 3.7 ± 0.32 nm along the *X* direction and 3.5 ± 0.28 nm along the *Z* direction (simulation **IR2**). Continuation of the simulation **IR2** for additional 15 ns did not result in any significant changes in the system; the lipid assembly contacts its periodic image along two directions and the degree of water contacts along the third direction remains essentially constant.

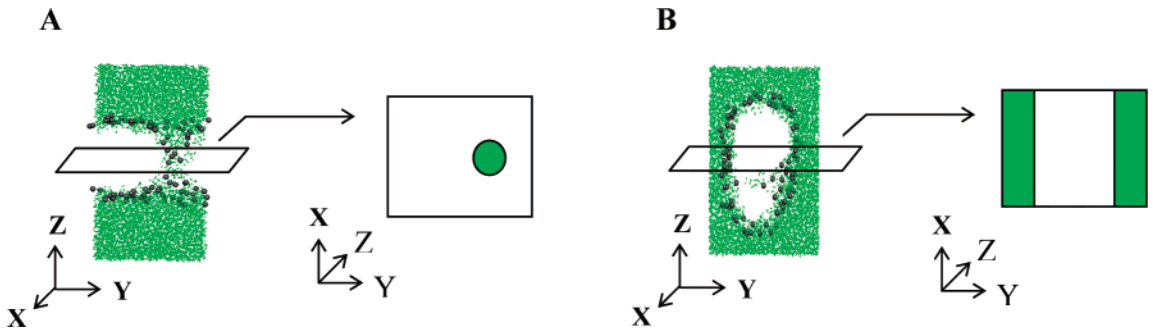

Figure 2. Schematic of the cross section of the simulation box viewed along the *Z* direction for simulation **AR1**; the view is for the 7 ns time point (panel A). For comparison, a similar schematic is shown for simulation **IR1** (2 ns time point; panel B). This schematic brings out the difference in the nature of the aggregate formed in these two simulations.

Although the lipid molecules have rearranged to a lamellar-like structure with a water channel, it is unlikely that further simulation will result in a bilayer structure devoid of water channel because of isotropic pressure coupling. For the bilayer to form, the water molecules constituting the water channel will have to move to the region occupied by the water phase (i.e., along the *Y* direction), with the concomitant closing-in of the DPPC molecules. This requires that the box size decrease along the *X* and *Z* directions (in simulation **IR2**) so that the DPPC molecules can come together; simultaneously, the box size has to increase in the *Y* direction to accommodate the additional water molecules. Such an independent scaling of the three sides of the simulation box is not possible because of the isotropic pressure coupling, but possible with anisotropic (possibly semi-isotropic also) pressure coupling.

Evolution of the System with Initially Randomly Oriented DPPC Molecules with Anisotropic Pressure Coupling. In simulation **AR1**, after the rapid separation of hydrophobic and hydrophilic groups, the box size along the *Z* direction increases (3−3.5 nm; Figure S2) independent of other two directions. This independent scaling is possible due to the anisotropic nature of pressure coupling. Rearrangement of the lipid molecules accompanied by fluctuations in box size led to the formation of lipid−lipid contacts along two directions (for example, along the *X* and *Y* directions in simulation **AR1**) and lipid−water contacts along the other direction (Figure 1B). These lipid−lipid and lipid−water contacts are consolidated with further simulation. After ∼4−6 ns, a lamellar structure is formed with a water channel (Figure 2). The independent scaling of the box size helps in the subsequent narrowing of the water channel by expulsion of the water molecules from the hydrophobic core. The DPPC molecules aggregate into a bilayer structure. The distribution of DPPC molecules in the two monolayers is almost equal (48 and 50 DPPC molecules). The size of the simulation box remains essentially constant in all the three directions once the bilayer is formed completely, i.e., from 15 ns onward up to the end of simulation (Table S2).

The system evolves in a similar fashion in the other four simulations, **AR2** (Figure 1F) to **AR5**. However, the water channel disappears completely in only simulation **AR1** (Figure 1A). An earlier simulation study by Marrink et al., on the self-assembly of 64 DPPC molecules also found that the lipid molecules rearrange rapidly to form a bilayer with a water channel; however, the water channel persists for variable durations (10−100 ns) in different simulations.[17] In view of this, it is possible that continuation of simulations **AR2**−**AR5** would eventually lead to the disappearance of the water channel.

The initial size of the box used in simulation **AR1** is bigger along the *Z* direction than along *X* or *Y* directions. This led to the formation of a bilayer with bilayer-normal parallel to the *Z* axis. The other four simulations were initiated in a cubic box and hence, there is no bias in the orientation of the bilayer. This led to the formation of bilayer with its normal parallel to the *X* axis in simulation **AR5**, to the *Y* axis in simulation **AR4** and to the *Z* axis in simulations **AR2** and **AR3**.

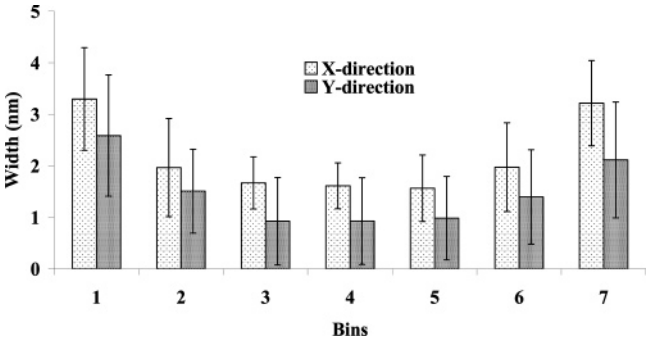

Figure 3. Bar diagram depicting the variations in the width of the water channel in the *X* and *Y* directions in simulation **AR1**. The water channel along the *Z* direction was divided in to seven equal bins and the width was calculated as the difference between the maximum and minimum values of the *X* coordinates (or *Y* coordinates) of all the water molecules within that bin. The values are averages for the duration from 10 to 15 ns of simulation.

Characterization of the Water Channel Formed in Simulation AR1. A water channel precedes the formation of final aggregation state and persists for ∼10 ns in simulation **AR1**. The formation of such a water channel during the self-assembly of DPPC molecules has been observed previously also.[17] The water channel resembles an hourglass, being narrowest in the middle and widest at the top (Figure 3). The channel is wider along the *X* direction (∼1.6 and ∼3.3 nm in the middle and at the ends, respectively) than along the *Y* direction (∼0.9 and ∼2.6 nm). The water channel first constricts in the middle and squeezes out the water molecules in both the *Z* directions within a short time. The channel disappears completely at ∼15 ns.

The water molecules in the water channel are dynamic. Some water molecules traverse through the water channel from one side of the bilayer to the other side whereas others enter and exit the channel from the same side (Figure 4). The time taken by different water molecules to traverse the water channel varies from ∼0.03 to ∼3.4 ns with an average time of 1.4 ± 0.8 ns (Figure 5). Water molecules that enter and exit the water channel from the same side of the bilayer have an average lifetime of 1.3 ± 0.7 ns with a maximum of 3.7 ns (water molecules that remain in the channel for less than 0.5 ns have not been considered).

The simulation **AR1** was continued for a further period of 10 ns after the disappearance of the water channel and the concomitant formation of the final aggregation state. No

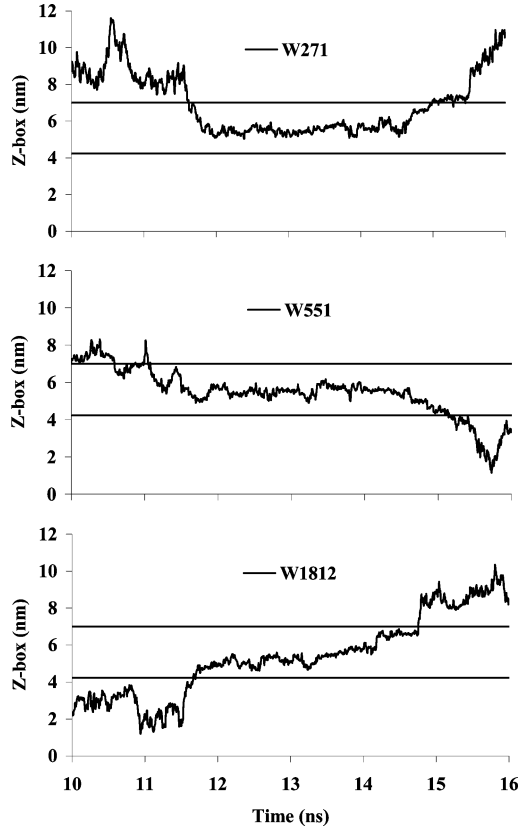

Figure 4. Dynamics of water molecules constituting the water channel for simulation **AR1**. Variations in the *Z* coordinates of the oxygen atoms of three representative water molecules that constitute the water channel are shown as a function of time. Water molecules **W551** and **W1812** move from one side of the bilayer to the other; water molecule **W271** exits the water channel from the same side as it entered. The horizontal lines indicate the approximate boundaries of the hydrophobic core of the bilayer (as deduced from the electron density profile of methylene carbon atoms).

significant changes are observed in the DPPC aggregates during this period. The system properties sample steady values during this period.

Analysis of Bilayer Characteristics. The trajectory data for the period 16−26 ns from simulation **AR1** were analyzed for characterizing the DPPC bilayer. The results were compared with those obtained from simulations of preformed bilayers (configuration **BN** and **BI**) performed with isotropic (simulation **IBN** and **IBI**) or anisotropic (simulations **ABN** and **ABI**) pressure coupling and with the results from the experimental and simulation studies reported in the literature.

Electrostatic Potential. The variation in the total electrostatic potential along the *Z* axis calculated from simulation **AR1** is nearly same as that obtained from the other four bilayer simulations (Figure 6). The phospholipids have a positive potential, and the water phase has a negative potential. The variations in the individual electrostatic potentials for phospholipid and water molecules are small. The general pattern of variation of the water, phospholipid, and total electrostatic potentials obtained in the present study is very similar to those reported by earlier MD simulation studies of hydrated DPPC bilayers.[19,21,33]

The Electron Density Profiles. These were computed from simulation **AR1** for the methylene, methyl and carbonyl groups, phosphorus and nitrogen atoms, and water (Figure 7). From the profiles of the carbonyl group and water, it is evident that water penetrates up to the carbonyl groups and is excluded from the hydrophobic core made of the methyl and methylene groups. The profiles of the methylene and carbonyl groups partly overlap with each other. The hydrophobic region starts after the carbonyl groups and thus, the carbonyl group peak-to-peak distance (Table 2) gives an indirect measure of the thickness of the hydrophobic core.

The Distribution of N Is Broader Than That of P, Reflecting Higher Conformational Freedom of Lipid Nitrogen. The difference in peak to peak distances for phosphorus and nitrogen is small (Figure 7 and Table 2). Thus, the P → N vector prefers an orientation that is parallel to the bilayer plane (Figure S3) as has been reported earlier from the neutron diffraction studies of DPPC.[34] Superposition of the electron density profiles obtained from the five simulations **AR1**, **ABI**, **ABN**, **IBI**, and **IBN** shows that the distributions remain very

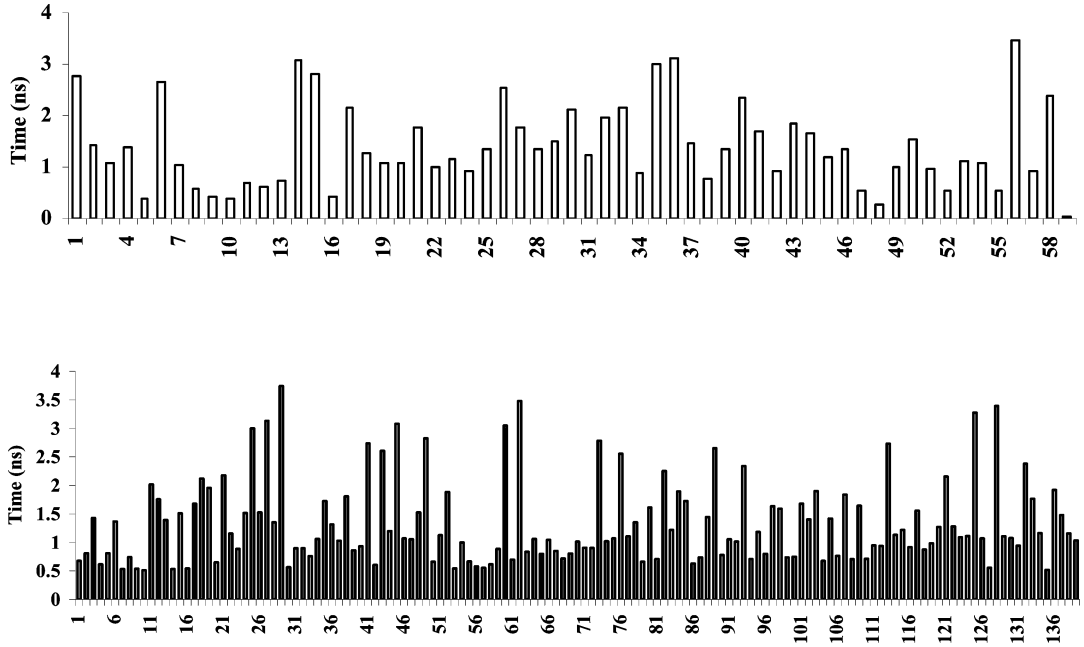

Figure 5. Transit times of the 59 water molecules that traverse the water channel from one side to the other (top panel) and the time spent in the water channel by the 141 water molecules that enter, remain in the water channel for at least 0.5 ns and exit from the same side (bottom panel) in simulation **AR1**.

TABLE 2: Comparison of the Bilayer Characteristics Derived from This Study with Those Reported in the Literature[a]

	simulation					
	isotropic pressure coupling		anisotropic pressure coupling			
bilayer/DPPC characteristics	IBN	IBI	ABN	ABI	AR1	lit. values
peak to peak distance (nm)						
carbonyl	3.2	3.0	3.0	3.0	3.1	
methylene	1.8	1.8	1.8	1.8	1.8	
P	4.1	4.0	3.9	3.9	4.0	3.7[e]
N	4.2	4.3	4.0	4.1	4.0	
D_{HH}	3.6	3.6	3.7	3.7	3.7	3.8[f]
interfacial width[b]	1.2	1.1	1.2	1.1	1.2	1.0−1.3[g]
av surface area per lipid (nm^2)	0.59	0.59	0.61	0.62	0.62	0.63 ± 0.01[h]
av vol of the bilayer (nm^3)	1.21	1.19	1.20	1.20	1.20	1.23[f]
area compressibility modulus (mN/m)[c]	107 545	109 618	1782	1223	628	231 ± 20[f]
av chain tilt (in deg) with respect to the *Z*-direction						
sn-1 (or γ) chain	29	28	30	30	30	
sn-2 (or β) chain	27	28	30	30	30	
av no. (%) in gauche conformation						
hydrocarbon C−C bonds	23	23	24	24	23	27−32[i] 23−46[j]
C2−C1−O−P[d]	5	7	6	6	5	
C1−O−P−O[d]	87	85	86	87	87	
O−P−O−C11[d]	75	74	74	71	69	
P−O−C11−C12[d]	4	4	4	4	4	
O−C11−C12−N[d]	64	66	64	65	62	

[a] From the 2−11 ns data of simulations **IBN**, **IBI**, **ABN**, and **ABI** and from the 16−26 ns data of simulation **AR1**. [b] Calculated from the electron density profile of water and was taken as the width of the region where the electron density of water is between 10 and 90% of bulk water.[19] [c] Calculated as suggested by Anezo et al.[20] [d] C1, C2 are atoms of the glycerol moiety; O, P are atoms of the phosphate group; C11, C12, and N are atoms of the choline headgroup. The atom nomenclature is following ref 52. [e] From X-ray scattering data of DPPC vesicles.[53] [f] From ref 8. [g] From ref 15. [h] From X-ray studies of fully hydrated L_α phase DPPC bilayers.[54] [i] From IR spectroscopic studies of DPPC bilayers.[38] [j] From deuterium magnetic resonance spectroscopic studies of DPPC bilayers.[36]

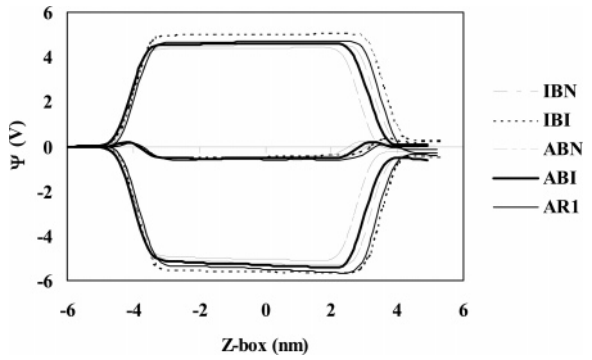

Figure 6. Variation of the electrostatic potential along the *Z* direction of the simulation box. *Z* box = 0 corresponds to the water phase. The upper half of the graph (i.e., positive values of on the ordinate of the graph) shows the electrostatic potential of phospholipids and the lower panel (i.e., negative values of on the ordinate) shows the electrostatic potential for the water molecules; the total electrostatic potential is in the middle. The potential was calculated using the *g_potential* module of the *GROMACS* analysis tool kit.

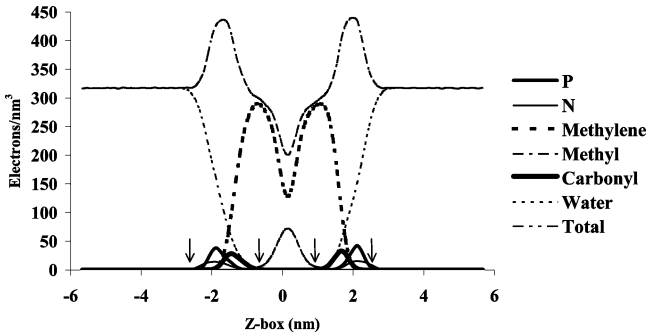

Figure 7. Electron density profiles of the phosphorus and nitrogen atoms, methylene, methyl and carbonyl groups and water computed from the simulation **AR1**. The total electron density profile is also shown. The center of the bilayer is 0 on the abscissa of the graph. The middle pair of arrows denotes the approximate points where the water densities become zero; the distances between these two points are 2.0, 1.8, 2.0, 1.9, and 1.4 nm in simulations **IBN**, **IBI**, **ABN**, **ABI**, and **AR1**, respectively. The outer pair of arrows denotes the approximate points where the nitrogen densities become zero; the distances between these two points are 5.6, 5.7, 5.5, 5.7, and 5.3 nm in simulations **IBN**, **IBI**, **ABN**, **ABI**, and **AR1**, respectively. The head-to-head distance D_{HH} (Table 2) is computed as the peak-to-peak distance in the total electron density profile. The densities were calculated using the *g_density* module of the *GROMACS* toolkit.

nearly the same irrespective of the nature of pressure coupling and the starting configuration (Figure S4).

The Values of Surface Area Obtained from Simulations Performed with Anisotropic Pressure Coupling Are Very Similar to Those Derived from Experimental Studies. Smaller values of surface area are obtained from simulations performed with isotropic pressure coupling (Table 2). The distribution of surface area values derived from **IBI** and **IBN** simulations is narrower than that derived from the other three simulations (Figure S5). In contrast, the average volume of the bilayer computed from simulations performed with anisotropic pressure coupling is intermediate to that obtained from simulations **IBI** and **IBN** (Table 2). The values are slightly less than that obtained from experiments.

The Area Compressibility Modulus Shows a Different Trend. The values are higher than those obtained from experiments in all the simulations; however, the deviations are extremely high ($>10^5$) when isotropic pressure coupling is used (Table 2). Such a deviation arising due to the inhibition of bilayer undulations as a result of small system size was also observed in the simulations of glycerolmonoolein and a lower area compressibility value was obtained by increasing the system size.[35] Isotropic pressure coupling does not allow the box to relax and this is required to accommodate undulations; this leads

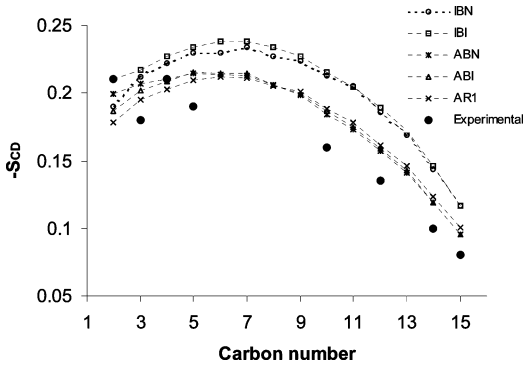

Figure 8. Deuterium order parameter (S_{CD}) of the hydrocarbon methylene groups calculated from all the five simulations along with the experimental values reported in the literature.[36] The values were computed using the *g_order* module of *GROMACS* toolkit.

to higher area compressibility modulus. The values obtained from the three simulations with anisotropic coupling (**ABN**, **ABI**, and **AR1**) are much lower (in the range 600−1800; Table 2) than those obtained from simulations with isotropic pressure coupling (**IBN** and **IBI**). The compressibility modules obtained from simulation **AR1** is the lowest and much closer to the experimentally observed value. A bilayer system consisting of 200 DPPC molecules was generated by appropriately replicating the bilayer of 98 DPPC molecules. This system was simulated for 9 ns with anisotropic pressure coupling. It was observed that the area compressibility modulus calculated from this simulation (622 mN/m) is similar to that obtained from simulation **AR1**.

Analysis of the Conformation of the Hydrocarbon Tails. The deuterium order parameter describes the motional disorder of the hydrocarbon chains and is higher for the methylene carbon atoms which are closer to glycerol (Figure 8). In contrast, atoms toward the chain terminus have lower values indicating that these atoms have no preferential orientation. The values are higher for all the carbon atoms when isotropic pressure coupling is used (simulations **IBN** and **IBI**); the values obtained from simulations performed with anisotropic pressure coupling (**ABN**, **ABI**, and **AR1**) are much closer to those reported from experimental[36] and simulations[29,37] studies.

The tilts of the two hydrocarbon chains with respect to the *Z* axis (Table 2) and their distributions (Figure S6) and the average number of C−C bonds adopting the gauche conformation are nearly the same whether isotropic or anisotropic pressure coupling is used. These values are similar to the lower end of range (23−46%; three to six gauche dihedrals per chain) obtained from deuterium magnetic resonance studies[36] but are lower than that (27−32%; 3.6−4.2 gauche dihedrals per chain) obtained from IR spectroscopic studies of DPPC bilayers.[38] A value of 25.5% was obtained from simulations of hydrated DPPC bilayer.[39] It has been reported that the fraction of gauche dihedral is less sensitive to ordering of the system unlike surface area.[39]

Analysis of the Conformation of the Choline Headgroup. The conformation of the choline headgroups (Table 2) and the orientations of the P → N vectors are not influenced by the nature of pressure coupling and agree well with those obtained from experimental studies.[34,40−42] The dihedrals C2−C1−O−P and P−O−C11−C12 are predominantly in the trans conformation whereas the dihedrals C1−O−P−O, O−P−O−C11 and O−C11−C12−N are predominantly gauche (Table 2). The P → N vector was found to be distributed mainly between 60 and 90° with respect to the bilayer normal (Figure S3).

Discussion

The spontaneous aggregation of DPPC molecules distributed and oriented randomly has been studied with isotropic and anisotropic pressure coupling in the present study. The results presented here show that the choice of the pressure coupling method determined the final aggregation state of DPPC molecules. Systems coupled anisotropically aggregated to a bilayer (or bilayerlike) following a similar mechanism except for the orientation of the bilayer in the simulation box. Systems coupled isotropically formed either a cylindrical micelle (simulations **IR1** and **IR4**) or stabilized as a lamellar structure with a large water channel (simulations **IR2**, **IR3**, and **IR5**). A water channel is also observed during the anisotropic simulation **AR1**, but the diameter of the water channel is much smaller than that found using the isotropic simulation **IR2**. Formation of a cylindrical micelle is probably due to the initial events of aggregation where lipid molecules lose contact with each other in two directions. The aggregates formed in simulations **IR2**, **IR3**, and **IR5** are similar to the aggregate formed in systems coupled anisotropically. However, to achieve a bilayer configuration, the subsequent narrowing of water channel is needed. This narrowing is achieved only when one of the box size increases and either both or one of the other two axes decreases. Such an independent scaling is not possible for system coupled isotropically but possible for system coupled anisotropically.

The formation of a micellar aggregate is unrealistic since it has been shown from ^{31}P NMR spectroscopic studies that PCs having hydrocarbon tails with nine or more carbon atoms form bilayers only.[43] Thus, the formation of cylindrical micelle can be considered as an artifact of isotropic pressure coupling. Use of isotropic pressure coupling also led to lower surface area and higher order parameter compared to anisotropic pressure coupling when simulations were started with preformed bilayers. The data from simulations using anisotropic pressure coupling are in better agreement with those reported from earlier experimental and simulation studies.[21,31]

Berendsen's weak coupling algorithm[32] has been used in the present study to maintain the pressure constant. This algorithm has also been used in many other lipid simulation studies reported in the literature (see, for example, refs 23, 39, and 44). A constant pressure can also be achieved by the use of other algorithms such as Andersen,[45] Parrinello−Rahman,[46] Nose−Hoover,[47] etc. Bond et al.[48] studied the spontaneous formation of DPC micelles around the *Escherichia coli* outer membrane protein OmpA and around glycophorin A from red blood cells. The results were compared with simulations of preformed micelles containing the respective proteins. For the simulations of OmpA-containing micelle, Berendsen's algorithm was used whereas for the simulations of glycophorin A, Parrinello−Rahman's algorithm was used. In both cases, the end-structures of self-assembled OmpA and glycophorin A micelles were found to be remarkably similar to their preformed counterparts.[48] Anezo et al.[20] studied the structure and dynamics hydrated DPPC using Parrinello−Rahman or Berendsen algorithms for maintaining the constant pressure; it was observed that the equilibrium properties of the DPPC bilayer are not much affected by the choice of pressure coupling algorithm.

There have been many studies on the spontaneous aggregation of lipids by complete atomistic[16,17,22,24,25] and coarse grain[18,23,26] simulations (Table S3). The spontaneous aggregation of surfactants around proteins has also been simulated.[48,49] The typical aggregation process occurs in nanosecond time scale and is ∼15 ns for bilayers, 5−10 ns for micelles and reverse micelles, and ∼90 ns for small vesicles. The aggregation process, although

varying in time scale, follows more or less the same pathway: rapid separation of the hydrophobic and hydrophilic regions followed by the formation of the aggregate. An intermediate step, wherein lipids cluster in to small groups is observed during the formation of micelles and vesicles.[16,18,25] One important characteristic observed during the aggregation into bilayer or vesicle is metastable water channel/pore, which was found to be rate limiting for the formation of final aggregate.[17,22] The dynamics of such pores during the aggregation process is not well understood, although the pores are stabilized using applied surface tension and studied.[50] In this study, we have characterized the water channel in terms of its diameter and the dynamics of the constituent water molecules.

Acknowledgment. R.Y.P. thanks the Indian Institute of Technology Bombay for a research fellowship. The authors thank Prof. Y. U. Sasidhar, Department of Chemistry for helpful discussion. This work was supported by a grant from the Council of Scientific and Industrial Research, India to P.V.B. under the NMITLI scheme (5/258/10/2002-NMITLI).

Abbreviations Used

DAPC	diacylphosphatidylcholine
DOPC	dioleoylphosphatidylcholine
DOPE	dioleoylphosphatidylethanolamine
DPC	dodecylphasphatidylcholine
DPPC	dipalmitoylphasphatidylcholine
MD	molecular dynamics
PME	particle mesh Ewald

Supporting Information Available: Additional data about the simulations, where Table S1 provides data about the distribution of the DPPC molecules in the five random configurations, **R1**−**R5**, Table S2 contains the average box size (along with standard deviation) and the box size in the last frame of the simulation, Table S3 is a summary of the some reported studies on the spontaneous assembly of lipids, Figure S1 shows the ball-and-stick representations of the two initial bilayerlike configurations, and the variation of the box size and the characterization of the bilayer are given in Figures S2−S6. This material is available free of charge via the Internet at http://pubs.acs.org.

References and Notes

(1) Arora, A.; Tamm, L. K. *Curr. Opin. Struct. Biol.* **2001**, *11*, 540−547.
(2) Gawrisch, K.; Eldho, N. V.; Polozov, I. V. *Chem. Phys. Lipids.* **2002**, *116*, 135−151.
(3) Hamilton, J. A. *Prog. Lipid Res.* **2004**, *43*, 177−199.
(4) Kahya, N.; Scherfeld, D.; Bacia, K.; Schwille, P. *J. Struct. Biol.* **2004**, *147*, 77−89.
(5) Lee, A. G. *Biochim. Biophys. Acta* **2003**, *1612*, 1−40.
(6) Maier, O.; Oberle, V.; Hoekstra, D. *Chem. Phys. Lipids.* **2002**, *116*, 3−18.
(7) Milhaud, J. *Biochim. Biophys. Acta* **2004**, *1663*, 19−51.
(8) Nagle, J. F.; Tristram-Nagle, S. *Biochim. Biophys. Acta* **2000**, *1469*, 159−195.
(9) Rinia, H. A.; de Kruijff, B. *FEBS Lett.* **2001**, *504*, 194−199.
(10) Tristram-Nagle, S.; Nagle, J. F. *Chem. Phys. Lipids.* **2004**, *127*, 3−14.
(11) Ash, W. L.; Zlomislic, M. R.; Oloo, E. O.; Tieleman, D. P. *Biochim. Biophys. Acta*, **2004**, *1666*, 158−189.
(12) Chiu, S. W.; Jakobsson, E.; Mashl, R. J.; Scott, H. L. *Biophys. J.* **2002**, *83*, 1842−53.
(13) Saiz, L.; Bandyopadhyay, S.; Klein, M. L. *Biosci Rep.* **2002**, *22*, 151−173.
(14) Scott, H. L. *Curr. Opin. Struct. Biol.* **2002**, *12*, 495−502.
(15) Tieleman, D. P.; Marrink, S. J.; Berendsen, H. J. C. *Biochim. Biophys. Acta* **1997**, *1331*, 235−270.
(16) de Vries, A. H.; Mark, A. E.; Marrink, S. J. *J. Am. Chem. Soc.* **2004**, *126*, 4488−4489.
(17) Marrink, S. J.; Lindahl, E.; Edholm, O.; Mark, A. E. *J. Am. Chem. Soc.* **2001**, *123*, 8638−8639.
(18) Marrink, S. J.; Mark. A. E. *J. Am. Chem. Soc.* **2003**, *125*, 15233−15242.
(19) Tieleman, D. P.; Berendsen, H. J. C. *J. Chem. Phys.* **1996**, *105*, 4871−4880.
(20) Anezo, C. A.; de Vries, H.; Holtje, H. D.; Tieleman, D. P.; Marrink, S. J. *J. Phys. Chem. B.* **2003**, *107*, 9424−9433.
(21) Patra, M.; Karttunen, M.; Hyvonen, M. T.; Falck, E.; Lindqvist, P.; Vattulainen, I. *Biophys. J.* **2003**, *84*, 3636−3645.
(22) de Vries, A. H.; Mark, A. E.; Marrink, S. J. *J. Phys. Chem. B.* **2004**, *108*, 2454−2463.
(23) Goetz, R.; Lipowsky, R. *J. Chem. Phys.*, **1998**, *108*, 7397−7409.
(24) Lu, L.; Berkowitz, M. L. *J. Am. Chem. Soc.* **2004**, *126*, 10254−10255.
(25) Marrink, S. J.; Tieleman, D. P.; Mark, A. E. *J. Phys. Chem. B.* **2000**, *104*, 12165−12173.
(26) Yamamoto, S.; Maruyama, Y.; Hyodo, S. *J. Chem. Phys.* **2002**, *116*, 5842−5849.
(27) Berendsen, H. J. C.; van der Spoel, D.; van Drunen, R. *Comput. Phys. Comm.* **1995**, *91*, 43−56.
(28) Lindahl, E.; Hess, B.; van der Spoel, D. *J. Mol. Mod.* **2001**, *7*, 306−317.
(29) Berger, O.; Edholm, O.; Jahnig, F. *Biophys. J.* **1997**, *72*, 2002−2013. www.ucalgary.ca/~tieleman/files/lipid.itp.
(30) Chiu, S. W.; Clark, M.; Balaji, V.; Subramaniam, S.; Scott, H. L.; Jakobsson. E. *Biophys. J.* **1995**, *69*, 1230−1245.
(31) Patra, M.; Karttunen, M; Hyvonen, M. T.; Falck, E.; Vattulainen, I. *J. Phys. Chem. B.* **2004**, *108*, 4485−4494.
(32) Berendsen, H. J. C.; Postma, J. P. M.; van Gunsteren, W. F.; DiNola, A.; Haak, J. R. *J. Chem. Phys.* **1984**, *81*, 3684−3690.
(33) Shinoda, W.; Shimizu, M.; Okazaki, S. *J. Phys. Chem. B.* **1998**, *102*, 6647−6654.
(34) Buldt, G.; Gally, H. U.; Seelig, A.; Seelig, J.; Zaccai, G. *Nature (London)* **1978**, *271*, 182−184.
(35) Marrink, S. J.; Mark, A. E. *J. Phys Chem B.* **2001**, *105*, 6122−6127.
(36) Seelig, J.; Seelig, A. *Biochemistry* **1974**, *13*, 4839−4845.
(37) Chandrasekhar, I.; Kastenholz, M.; Lins, R. D.; Oostenbrink, C.; Schuler, L. D.; Tieleman, D. P.; van Gunsteren, W. F. *Eur Biophys. J.* **2003**, *32*, 67−77.
(38) Mendelsohn, R.; Davies, M. A.; Brauner, J. W.; Schuster, H. F.; Dluhy, R. A. *Biochemistry* **1989**, *28*, 8934−8939.
(39) Hofsass, C.; Lindahl, E.; Edholm, O. *Biophys. J.* **2003**, *84*, 2192.
(40) Akutsu, H. *Biochemistry* **1981**, *20*, 7359−7366.
(41) Akutsu, H.; Nagamori, T. *Biochemistry* **1991**, *30*, 4510−4516.
(42) Seelig, J.; Gally, G. U.; Wohlgemuth, R. *Biochim. Biophys. Acta* **1977**, *467*, 109−119.
(43) Kleinschmidt, J. H.; Tamm, L. K. *Biophys. J.* **2002**, *83*, 994−1003.
(44) Lindahl, E.; Edholm, O. *Biophys. J.* **2000**, *79*, 426−433.
(45) Andersen, H. C. *J. Chem. Phys.* **1980**, *72*, 2384.
(46) Parrinello, M.; Rahman, A. J. *Appl. Phys.* **1981**, *52*, 7182.
(47) Martyna, G. J.; Tobias, D. J.; Klein, M. L. *J. Chem. Phys.* **1994**, *101*, 4177.
(48) Bond, P. J.; Cuthbertson, J. M.; Deol, S. S.; Sansom, M. S. P. *J. Am. Chem. Soc.* **2004**, *126*, 15948−15949.
(49) Braun, R.; Engelman, D. M.; Schulten, K. *Biophys. J.* **2004**, *87*, 754−763.
(50) Leontiadou, H.; Mark, A. E.; Marrink, S. J. *Biophys. J.* **2004**, *86*, 2156−2164.
(51) Humphrey, W.; Dalke, A.; Schulten, K. *J. Mol. Graphics* **1996**, *14*, 33−38.
(52) Sundaralingam, M. *Ann. N. Y. Acad. Sci.* **1972**, *195*, 324−355.
(53) Lewis, B. A.; Engelman, D. M. *J. Mol. Biol.* **1983**, *166*, 211−217.
(54) Nagle, J. F.; Zhang, R.; Tristram-Nagle, S.; Sun, W.; Petrache, H. I.; Suter, R. M. *Biophys. J.* **1996**, *70*, 1419−1431.